CHIMIA 49 (1995) Nr. 1/2 (Januar/Februar)

Chimia 49 (1995) 17–22

ISSN 0009–4293

Preparation and Characterization of Mixed-Oxide Electrocatalysts Based on RuO_2 and IrO_2

Achille De Battisti*, **Giancarlo Battaglin**[a]), **Alvise Benedetti**[a]), **Janos Kristof**[b]), and **Janos Liszi**[c])

Abstract. The formation processes of RuO_2/TiO_2, IrO_2/TiO_2 and IrO_2/ZrO_2 film electrodes have been studied by combined thermoanalytical and mass-spectrometric methods. The obtained materials have been characterized by cyclic voltammetry (CV). The precursor path leading to mixed oxides for the first two groups of materials, consists of several stages, including solvent desorption, oxidative cracking, combustion, noble-metal chloride decomposition. Minima of the temperature of chlorine release and organic combustion have been observed for precursor salt mixtures with intermediate-low noble-metal concentrations. The microstructural investigation, carried out by wide-angle X-ray scattering (WAXS) has shown that solid solutions are formed within quite wide composition ranges for TiO_2-stabilized materials. For the IrO_2/ZrO_2 system, segregation of amorphous ZrO_2 takes place for IrO_2 concentrations ≤ 80 mol-%. For the TiO_2-stabilized samples, the characterization by cyclic voltammetry has shown that maxima of charge-storage capacity are observed for those electrodes whose composition is in the range of minimum temperature for the precursor reaction. A dependence of the faradaic voltammetric charge on the carbon content of the electrode films, as determined by nuclear reaction analysis (NRA), has been shown. The experimental results have been explained hypothesizing that minima of pyrolysis temperature involve less favorable conditions for rearrangements in the reacting films, and, consequently, larger degree of defectivity. In the case of IrO_2/ZrO_2 electrodes, the segregation of the amorphous ZrO_2 phase seems to be main reason for the maximum of charge-storage capacity observed at 80 mol-% of IrO_2.

1. Introduction

The increasing demand for efficient and stable electrodes in industrial processes like galvanics, wastewater treatment, organic electrosynthesis, hydrogen evolution, has prompted several researches on the optimization of electrode composition and parameters of the preparation. Most of the available literature concerns relatively simple systems based on one component (RuO_2 or IrO_2), or quasi-binary systems with formation of solid solutions [1–4]. More recently, the research has been extended to more complex materials, where components like ZrO_2 and Ta_2O_5 have also been taken into account, as stabilizers of the catalytically active component (RuO_2, IrO_2) [5–11]. These cases are very important for the practical application as stable anodes for oxygen evolution. They also supply a wide variety of miscibility between the oxide components useful to investigate the changes generated by the degree of dispersion of the catalytically oxide in parameters of the electrochemical performance, like electrocatalytic activity and wear-resistance. In [5][6][11], it has been shown that maxima of charge-storage capacity for RuO_2/ZrO_2, RuO_2/Ta_2O_5, IrO_2/ZrO_2, IrO_2/Ta_2O_5 are attained for intermediate noble-metal concentrations. In the same papers, interesting differences have been illustrated, between the properties of the above oxide mixtures, compared with the TiO_2-stabilized ones. In the present work, results are reported on the formation of RuO_2/TiO_2 and IrO_2/TiO_2 mixed oxide films, by pyrolysis of mixtures of ruthenium and iridium hydrated chlorides with $(i\text{-PrO})_2$Ti bis(pentane-2,4-dionate) (TIP), respectively. In this part of the research, thermoanalytical techniques combined with mass-spectrometry have been used. As far as the compositional features of the final oxide mixtures are concerned, *Rutherford* Backscattering Spectrometry (RBS) and NRA have been used, together with Elastic Recoil Detection (ERD) for hydrogen determination and concentration-depth profiling. The microstructural characterization has been carried out by WAXS. With the same methodology, IrO_2/ZrO_2 films have been characterized, and the properties compared with those of the other groups of materials. Investigation by cyclic voltammetry has been carried out in order to find correlations between the features of the precursor reactions, the final composition, and the electrochemical properties of the materials obtained.

2. Experimental

2.1. *Sample Preparation*

For RBS, NRA, ERD, WAXS, and electrochemical investigations, RuO_2/TiO_2 (20, 30, 50, 70, 80, 100 mol-% of noble-metal) and IrO_2/TiO_2 coatings (same compositions) were prepared on Ti plates (1 x 1 cm, thickness 0.3 mm). The films for thermoanal. investigation were prepared on Ti strips (4 x 12 mm, thickness 0.1 mm). The latter were previously etched by 20% oxalic acid at a temp. of 80°. Equimolar solns. of $RuCl_3 \cdot 3H_2O$, $IrCl_3 \cdot 3H_2O$, $(i\text{-PrO})_2$Ti bis(pentane-2,4-dionate) in i-PrOH were used for deposition of precursor salt films. In the case of thermoanal. investigations, loadings of 5–10 mg of precursor salt mixtures were transferred onto Ti strips. The preparation procedure of samples for electrochemical experiments was substantially similar to that above outlined.

2.2. *Thermoanalytical Experiments*

Thermoanal. investigations have been carried out by means of a derivatograph (*Hungarian Optics*, C-type instrument). Experiments were performed under O_2. The heating rate was 5° min^{-1} with isothermal stages at 400, 450, 500° (duration of 20 min each). Thermoanal./mass spectrometric (TG-MS) experiments were carried out with a *Perkin-Elmer* TGS-2/system 4 thermobalance, coupled with a *Balzers* QMG 511-type mass spectrometer. A cross-beam ion

*Correspondence: Prof. A. De Battisti
Dipartimento di Chimica dell'Università
Via L. Borsari, 46
I–44100 Ferrara
[a]) Unità CISM
Dipartimento di Chimica Fisica
dell'Università
I–30123 Venezia
[b]) Department of Analytical Chemistry of the University
H–8200 Veszprém
[c]) Department of Physical Chemistry of the University
H–8200 Veszprém

source operated at 70 eV electron energy was applied. Heating rate was 10° min^{-1} in these cases.

2.3. *Wide Angle X-Ray Scattering (WAXS)*

X-Ray spectra were collected using a *Philips* vertical Goniometer connected to a highly stabilized generator. Cu-K_α Ni-filtered radiation, a graphite monochromator, and a proportional counter with a double pulse-height discriminator were used. A step-by-step technique was employed: steps were of 0.05° with an accumulation counting time of 100 s per angular abscissa. Further details are described in [12].

2.4. *Ion-Beam Nuclear Techniques*

As mentioned in the *Introduction*, nuclear methods for surface analysis have been used. The details about RBS experiments for other sets of RuO_2/TiO_2 and IrO_2/TiO_2 electrode films have been reported in [13] and [14], respectively. For the determination of C content in RuO_2-based films the nuclear reaction has been applied, $^{12}C(d,p)^{13}C$. The energy of the deuteron beam was 620 keV, the detection angle was 150°.

2.5. *Electrochemical Measurements*

Cyclic voltammetry experiments were carried out by a *Solartron* 1286 electrochemical interface. Electrodes were tested in 1M $HClO_4$. The potential sweep range was 0.00–1.20 V (*vs.* S.C.E.). The voltammograms were recorded at different potential scan rates in the range 0.010–0.300 V s^{-1}.

3. Results and Discussion

3.1. *Study of the Precursor Path for TiO_2-Stabilized Films*

Thermoanalytical curves showed a complex thermolytic path for coatings of pure TIP. Four decomposition steps at 83, 163, 298, 445°, were detected. The DTG peaks at 163 and 298° can be due to the combustion of the organic complex. The corresponding DTA peaks indicate, in fact, exothermic processes at these temperatures. The peak at 83° is due to solvent removal, while that at 445° does not find a straightforward explanation. The results of the TG-MS experiments are in substantial agreement with the described observations, obtained at a lower heating rate. The ion-intensity curves, on the other hand, show the occurrence of cracking processes of the organic species, ill defined and extended over a relatively wide temperature range. The DTG and CO_2 ion intensity curve have the same shape, and all other ion intensity curves drop down to zero after the last decomposition step. These results indicate that the latter is associated with combustion of elemental carbon, residual of previous cracking processes. The thermoanalytical curves for the two pure noble-metal trichlorides have been also obtained. In the case of $RuCl_3 \cdot 3H_2O$ films, the thermolytic path seems more simple. A step connected with crystal water release is observed at 78°, while Cl_2 release seems to be associated with the weight loss at 354°. The thermoanalytical curves relative to $IrCl_3 \cdot 3H_2O$ films are quite more complex. Water release itself takes place between 20 and 260°. A mass loss amounting to only 7% of the total coating mass occurs at 369°. More substantial losses are observed at 453 and 494°, reasonably to be assigned to chloride final decomposition. The TG-MS curves indicate cracking of solvent species at lower temperatures, and a combustion in the range 260–500°, which is not easily explained, considering that the solvent should be eliminated at lower temperature, together with moisture. The presence of solvent molecules up to the combustion temperature can only be explained assuming that substitution of crystal water molecules by i-PrOH molecules takes place. The difference between the thermolytic paths of the two noble-metal salts justifies the significant differences in the microstructure of the final oxides obtained.

The mechanism of the pyrolysis for binary mixtures of precursor salts changes drastically with respect to those described for pure components. A decrease of the temperature of Cl_2 release for the noble-metal chloride and that of combustion for the organic ligands of the Ti complex are observed in particular. In the case of a precursor salt film containing 20 mol-% of Ru and 80 mol-% of Ti, *e.g.*, the combustion temperature is decreased of *ca.* 100°. The step at 445° in the TG curve for Ti complex alone, disappears. TG-MS Results on evolved gases indicate a better definition of the cracking processes occurring at lower temperature, in the range 100–300°. The range of the successive combustion stage is also more narrow, no CO_2 is evolved after the main combustion process. The case of Ir-based mixtures is substantially similar. For samples containing only 10 mol-% of iridium, the step at 445° in the TG curve for the pure Ti-precursor salt, due to the combustion of residual elemental carbon, disappears. Also in this case, the presence of the noble metal catalyzes both preliminary cracking and combustion of organic species. The chlorine elimination is accelerated, on the other hand, by the presence of the Ti salt and by its combustion. The thermoanalytical and mass spectrometric curves for

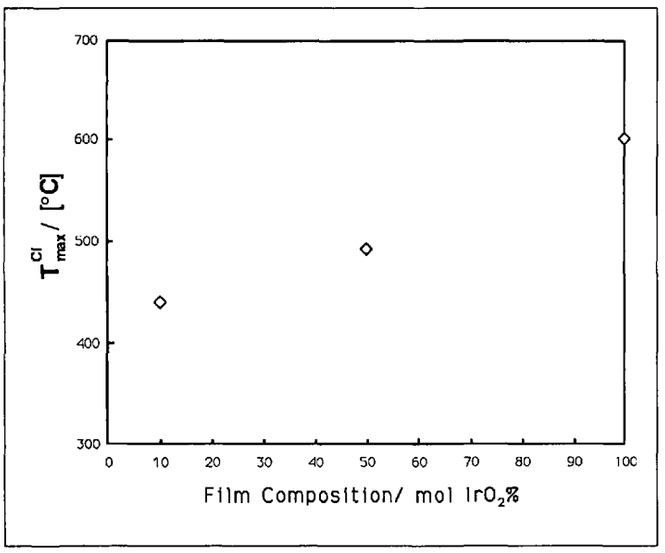

Fig. 1. *Dependence of the maximum chlorine release temperature on the film composition for a series of iridium(III) hydrated chloride/TIP mixtures*

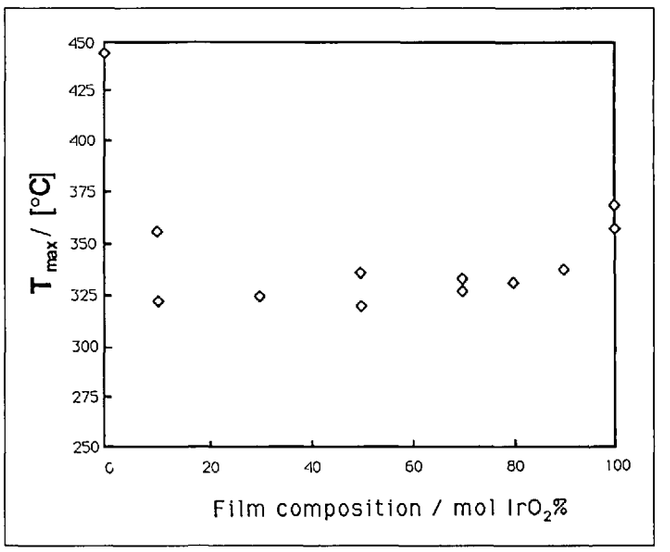

Fig. 2. *Maximum combustion rate temperature as a function of the film composition, for the same series of samples as shown in* Fig. 1

CHIMIA 49 (1995) Nr. 1/2 (Januar/Februar)

precursor salt mixtures with intermediate-high concentrations of noble metal substantially retain the main features of those above described. The Cl_2-elimination temperature, however, tends to increase with increasing the noble-metal content in the precursor salt mixture, as well as the maximum combustion temperature. The results are shown in *Figs. 1* and *2*, for the case of IrO_2/TiO_2 mixtures. The situation is analogous for Ru-based films. The most important aspect, deducible from the above results, is the considerable lowering of the temperature, at which the noble-metal chloride is decomposed, and the acceleration of the combustion process involving the organic components of the reaction mixture (solvent molecules, anions of the titanium complex). Both phenomena may cause larger degrees of porosity and microstructural defectivity in the residual solid intermediates, and, therefore, in the final oxides.

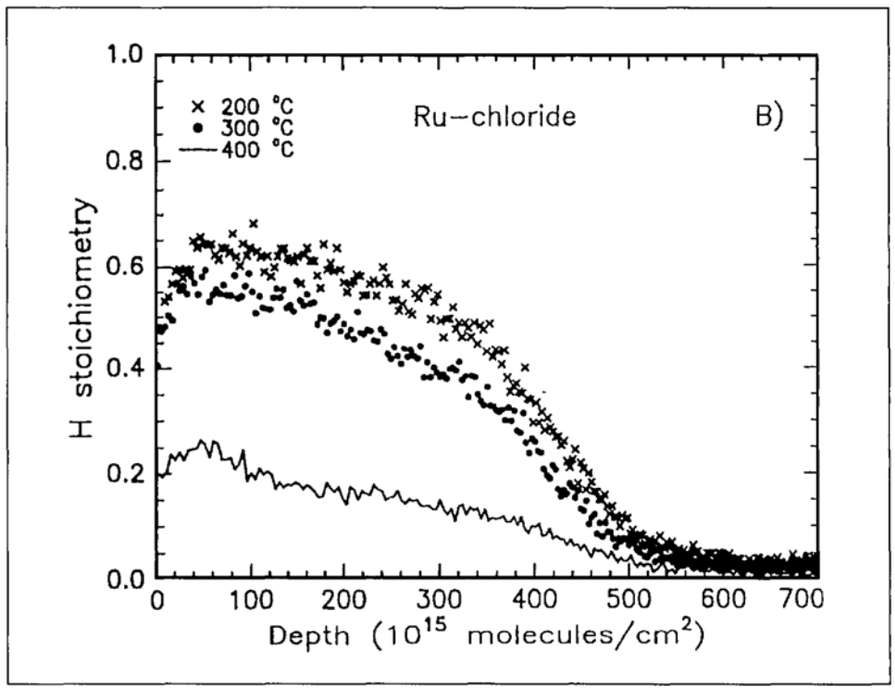

Fig. 3. *Hydrogen concentration profiles from ERD spectra for samples containing ruthenium hydrated chloride* (30 mol-%) *and TIP* (70 mol-%), *heated at 200, 300, 400°*

3.2. *RBS, NRA, ERD Results*

As far as the composition of the electrode films is concerned, RBS results confirmed segregation of TiO_2 species in the surface region of all the RuO_2/TiO_2 compositions. The same results have been found for IrO_2/TiO_2 [13] films and RuO_2/TiO_2 films containing 30 mol-% of noble-metal oxide [14]. As already commented in the above mentioned papers, this compositional anisotropy may induce additional microstructural defectivity. Making use of the ion-beam method based on the $^{12}C(d,p)^{13}C$ nuclear reaction, the content of residual carbon in RuO_2/TiO_2 films was determined. The results are reported in *Table 1*, in terms of C/Ru % atom fractions. A minimum of 11±3 atoms of C% has been found for the 100% RuO_2, a maximum of 35.8±9 at C%, for the 20 mol RuO_2% sample. Similar results were reported in [14] for different supported films containing 30 mol% of RuO_2, prepared from different Ru precursors. The significant amounts of residual carbon found in the oxide films are a further indication of the difficulty of the oxidation of organic components in the precursor mixture. In this light, the NRA data are a useful complement to the thermoanalytical results. Larger amounts of residual carbon at low-intermediate noble-metal concentrations in the supported oxide mixtures must be interpreted on the basis of the larger amounts of organics introduced together with the titanium precursor. The larger cracking and oxidation rates observed in the precursor mixtures of low-intermediate noble-metal contents do not seem to be sufficient to lead the combustion to completion. The amounts of residual hydrogen, as found by ERD, are close to the corresponding carbon contents. A typical concentration depth profile is shown in *Fig. 3*. The two residual species certainly have a common origin. The fact that their amounts are comparable is, therefore, not surprising. It can also be assumed that regions where hydrogen species enrichment is observed (near-surface region) are also characterized by carbon enrichment.

Table 1. *Residual Carbon Content of RuO_2/TiO_2 Films of Different Composition (Average of Three Samples)*

RuO_2 conc./mol-%	C/Ru at. ratio [%]
100	11 ± 3
80	12 ± 3
70	18 ± 4
50	12 ± 6
30	35 ± 10
20	33 ± 9

The analysis of the concentration/depth profiles of the IrO_2/ZrO_2 samples by RBS indicates some peculiar features. In *Fig. 4*, two RBS spectra are shown, relative to the samples containing 20 and 70 mol-% of IrO_2, respectively. For the former, it is easy to see that a layered structure is present, with IrO_2- and ZrO_2-rich regions alternating. The same shapes of spectra are observed for lower noble-metal concentrations. The spectrum of the 70 mol-% of iridium oxide, on the other hand, has a more conventional shape, indicating that some enrichment with ZrO_2 is present in the near-surface region. Samples with noble-metal concentrations ≥ 50 mol-% exhibit similar behavior. The combined RBS-NRA-ERD results indicate that the near surface region of mixed oxide films based on $RuO_2(IrO_2)/TiO_2$ mixtures becomes enriched with significant amounts of chemical and microstructural impurities. This factor influences in turn the surface texture of the films, and, therefore, the electrochemical properties. For the case of IrO_2/ZrO_2 system, although on the basis of a more limited amount of result, similar conclusions can be drawn, at least for IrO_2-rich films.

3.3. *WAXS Measurements*

On the basis of a more limited set of WAXS results shown in [14] and of more recent results obtained in the present research, it can be shown that a solid solution between RuO_2 and TiO_2 is formed. The dependence of the 2θ on the mixed oxide film composition is shown in *Fig. 5*, for the 110 reflection. A good linearity is observed, indicating that the formation of the solid solution does not involve microstructural anomalies. Nevertheless, the considerable amount of residual species from the preparation process, like carbon, hydrogen, and, as shown in other works [15], chlorine, the tetragonal rutile structure of the solid solution cannot be taken as representative of the whole sample.

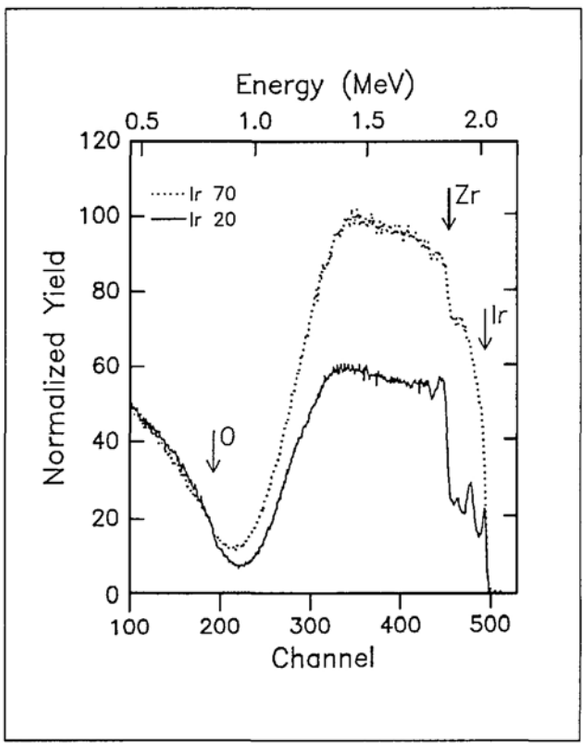

Fig. 4. *RBS Spectra for two IrO_2/ZrO_2 films containing 20 and 70 mol-% of IrO_2*

Table 2. *Average Crystallite Size* $< D >_v$ *Sizes* [Å] *Calculated from Different* hkl *Profiles Relative to the IrO_2 Phase*

Film composition/ mol IrO_2%	W-A pair 110–220	$<\varepsilon^2(L)^{1/2}$ [$\times 10^{-3}$]	110	101	211	002
100	56	10	40	58	38	41
80	140	8.1	106	108	70	128
70	145	9.3	108	122	63	131
50	156	8.8	120	141	61	120
30			104			
10			100			

Table 3. *Unit Cell Parameters of the Tetragonal IrO_2 and ZrO_2 Phases*

IrO_2 conc./mol-%	IrO_2 phase		ZrO_2 phase	
	a_0/Å	c_0/Å	a_0/Å	c_0/Å
100	4.547(2)	3.154(2)		
80	4.560(2)	3.165(3)		
70	4.571(4)	3.169(4)		
50	4.561(2)	3.168(2)		
30	4.562(2)	3.165(2)		
20			3.585(1)	5.148(4)
10			3.595(2)	5.158(5)
0			3.596(2)	5.162(6)
Literature	4.4983 [19]	3.1544 [19]	3.5961(2) [20]	5.1770(4) [20]

More likely, clusters of crystallites of the solid solution, generally defined as 'particles', are separated by wide regions were an amorphous character of the solid phase must prevail, and impurities are collected. This is somewhat witnessed by the compositional features of the near-surface region of the films, always enriched with impurities, and TiO_2. The anomalous effects of annealing time and temperature on the electrical resistivity of IrO_2 films observed in [15], at some extent the passivation phenomena observed during the thermolytic processes leading from hydrated $IrCl_3$ to IrO_2 [15–18], are indirect evidences of the same phenomenon already in one-component systems.

IrO_2/ZrO_2-mixed oxide electrodes exhibit interesting differences from those formerly described for the two above described TiO_2-stabilized materials. The microstructural investigation has shown, in particular, that formation of solid solution, if any, is restricted to the zirconia and iridia-rich ends of the composition coordinate. Although a tetragonal ZrO_2 phase is formed under the preparation conditions chosen in the present work, the features of the IrO_2 and ZrO_2 cells do not apparently allow a larger miscibility range. As shown in *Table 2*, the cell parameters of the 100% IrO_2 sample are significantly larger than the literature data [19] The change of IrO_2 cell parameters with lowering the IrO_2 concentration is rather complicated. The slight initial increase of a_0 and c_0 could be interpreted in terms of substitution of Ir^{IV} with Zr^{IV}. No significant change is observed above 30 mol-% of ZrO_2. The the values of a_0 and c_0 for the 100% ZrO_2 sample are quite close to the literature data [20]. The addition of the IrO_2 component causes a small decrease of both. Above 20 mol-% of IrO_2, however, the diffraction peaks assigned to tetragonal ZrO_2 phase disappear, and a halo between 27 and 32° becomes evident. Above the mentioned noble-metal oxide concentration, therefore, the zirconium precursor is converted into a microcrystalline-amorphous oxide phase, within which the IrO_2-rich phase particles are dispersed. A detailed microstructural investigation, carried out with the *Warren-Averbach* method, has shown, on the other hand that neither the microstrain in the crystallites, nor the average crystalllite size of the IrO_2-rich phase, is significantly affected by the sample composition (*Tables 3*). These microstructural features of the phase, containing the catalytically active component, are not particularly affected by changes in nominal composition of the electrode materials.

CHIMIA 49 (1995) Nr. 1/2 (Januar/Februar)

3.4. *Electrochemical Characterization*

Cyclic voltammograms at RuO_2/TiO_2, IrO_2/TiO_2, IrO_2/ZrO_2 electrode films have the common features of high background (capacitive) currents and the presence of a peak pair (anodic/cathodic), associated with the Ru^{IV}/Ru^{III} and Ir^{IV}/Ir^{III} redox couple, respectively.

The peak current i_p has been found to be linear in the potential scan rate s for RuO_2-based electrodes, in all the composition range explored (*Fig. 6*). The same feature is essentially retained also for the other two groups electrode films. For larger values of s, however, and for electrodes with larger charge-storage capacities, the exponent of s tends to be lower than 1.

Considering that all the electrode films studied in this work have been prepared with comparable total oxide loadings, a comparison of their charge-storage capacity can be made 'at constant thickness'. At constant s and composition, IrO_2-based materials show larger charge-storage capacity compared with those based on RuO_2. As shown in *Fig. 7*, on the other hand, among the former, the ZrO_2-stabilized electrodes have larger voltammetric charges. Following the scheme reported in [21], an evaluation of capacitive and faradaic contributions to the total charge storage capacity have been made. The peak (faradaic) charges of the electrodes stabilized with TiO_2 exhibit maxima around 20–30 mol-% of noble metal. For TiO_2 stabilized materials, with larger content of organics in the precursor mixtures, the thermolysis process is similar, and their CV features can be interpreted along the same lines. Voltammetric peak charges, a measure of the number of electroactive sites in the films, can be correlated with the microstructural defectivity. For electrode films prepared by pyrolysis of salts containing large amounts of organics (in our case RuO_2/TiO_2 and IrO_2/TiO_2 mixtures), the microstructural defectivity should also be monitored by the amount of residual carbon content. Accordingly, the correlation between the two parameters has been studied for a set of RuO_2/TiO_2 electrode films of different composition. Voltammetric peak charges have been normalized to the total amount of Ru+Ti atoms, as determined by RBS for each film. As expected, the normalized voltammetric peak charge at constant oxide loading increases with the carbon concentration, expressed as atom fraction C/Ru. The results on the thermoanalysis for the mechanism of the precursor path, NRA and RBS results on the compositional features of the final mixed-oxide products afford complementary explanations for the CV behavior of RuO_2/TiO_2 and IrO_2/TiO_2 film electrodes. Other aspects, like the segregation of TiO_2 (anatase) in the composition range, where the maxima of charge-storage capacity are observed [22], can also play a role. It has not been considered here explicitly at the moment. However, it can be an important factor contributing to increase the defectivity of the films. This aspect will be further discussed later.

As far as the IrO_2/ZrO_2 system is concerned, as mentioned in the *Experimental*,

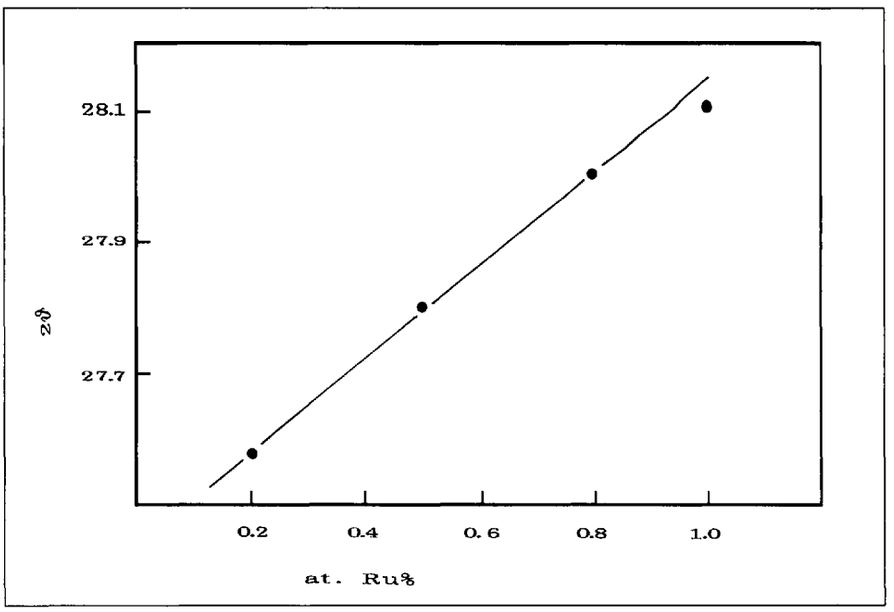

Fig. 5. *Dependence of 2θ for the 110 reflections on the film composition for a series of RuO_2/TiO_2 samples*

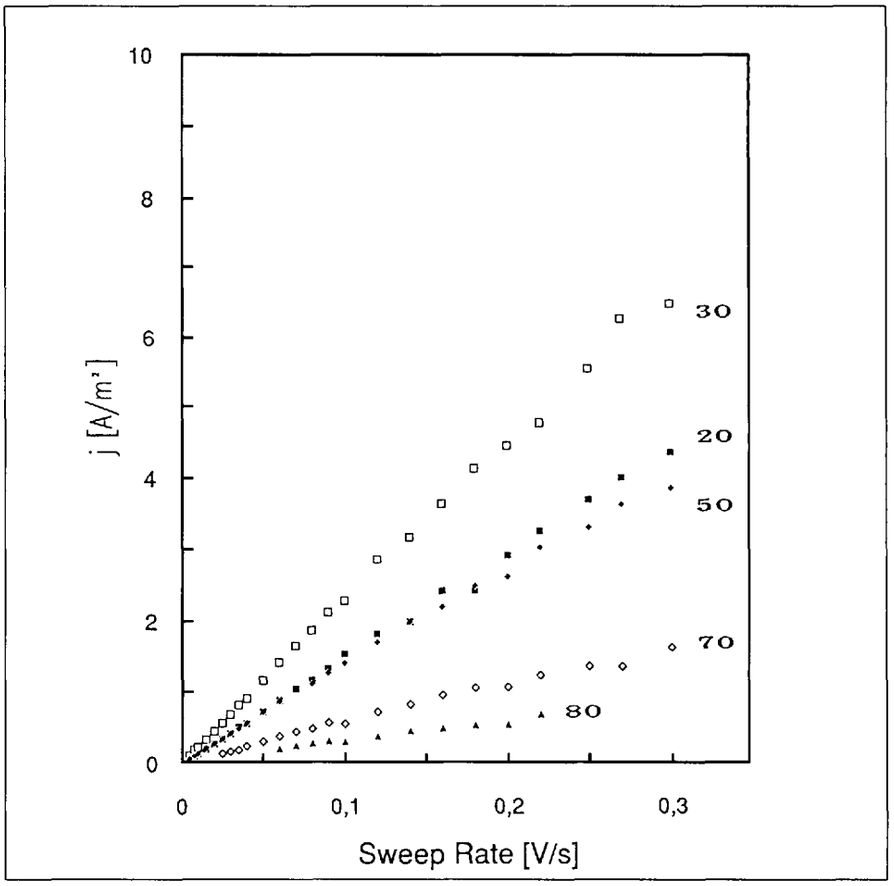

Fig. 6. *Dependence of the peak current density (i_p) on the potential sweep rate for a series of RuO_2/TiO_2 film electrodes.* The concentrations of RuO_2 in mol-% are reported in the *Fig.*

CHIMIA 49 (1995) Nr. 1/2 (Januar/Februar)

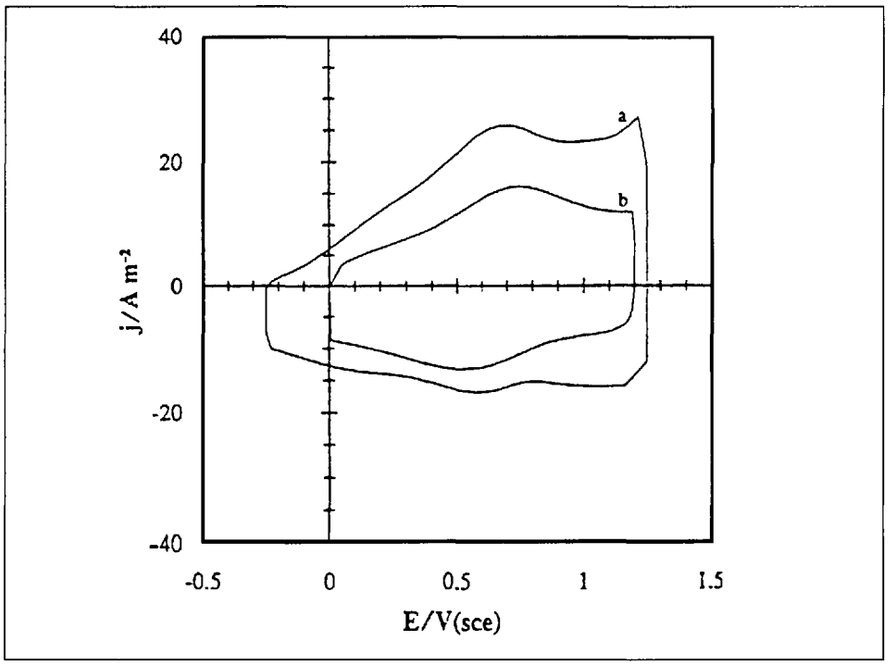

Fig. 7. *Comparison of voltammograms recorded in 1M $HClO_4$ at 0.100 V s^{-1} for:* a) *a IrO_2/ZrO_2 electrode film containing 30 mol-% of noble-metal oxide;* b) *a IrO_2/TiO_2 electrode film with the same noble-metal concentration as* a

no organic anions are present in the precursor salts. The only source of organic species, is in this case the solvent (i-PrOH), in which the precursors have been dissolved. In fact, preliminary TGA-DTA-EGA experiments have shown that the precursor path leading to the oxide mixture is relatively simpler than observed in the two former cases. In this case, the shape of the dependence of the voltammetric peak charge on the film composition is also somewhat simpler. The maximum is around 80 mol-% of noble-metal oxide. The lower charge-storage capacity of the 100% IrO_2 film can be interpreted assuming that in this case segregation of amorphous ZrO_2, occurring in the range of high IrO_2 concentrations, causes smaller size of the crystallite clusters (particles). The results obtained in the present work confirm the fact that IrO_2/ZrO_2 film electrodes have larger charge-storage capacities, compared with the TiO_2-stabilized ones [11]. Although the available microstructural data for such a wide set of materials are still insufficient, some tentative explanation can be proposed. In the case of the RuO_2/TiO_2 and IrO_2/TiO_2 films, the Ti precursor acts as the vehicle for a significant amount of hydrocarburic groups. The thermal and mechanic effects connected with their reactivity in the precursor mixture are larger just in the same composition range where anatase apparently begins to segregate. According to our results the combustion effect seems to dominate, but synergism of the two factors cannot be ruled out. In the case of the IrO_2/ZrO_2 films on the other hand, the organic components are supplied only by the solvent. The ZrO_2 phase, segregated below *ca.* 80 mol-% of IrO_2, seems to play in this case a quite effective role in increasing the roughness factor of the films. Its amorphous character apparently amplifies the intuitively important role of the segregation of a second phase.

Concluding, the results described in [5–11] about the electrochemical behavior and other physicochemical features of mixed-oxide electrodes, based on RuO_2 and IrO_2 electrocatalysts, and metal oxides of the groups IVB and VB as stabilizing componets, indicate the importance of the research in this field of electrocatalysis. Interesting possibilities of interpretation of some of the electrochemical evidence can be afforded, combining thermoanalysis, ion-beam nuclear methods for surface analysis and concentration/depth profiling, and X-ray diffractometric methods.

Received: October 20, 1994

[1] S. Trasatti, G. Lodi, in 'Electrodes of Conductive Metal Oxides', Ed. S. Trasatti, Elsevier, Amsterdam, 1980, Part A, p. 301.
[2] S. Trasatti, G. Lodi, in 'Electrodes of Conductive Metal Oxides', Ed. S. Trasatti, Elsevier, Amsterdam, 1981, Part B, p. 521.
[3] S. Trasatti, W.E. O'Gready, in 'Advances in Electrochemistry and Electrochemical Engineering', Eds. H. Gerischer and C.W. Tobias, Wiley, New York, 1981, Vol. 12, p. 177.
[4] D.M. Novak, B.V. Tilak, B.E. Conway, in 'Modern Aspects of Electrochemistry', Eds. B.E. Conway and J.O'M. Bockris, Plenum, New York, 1982, Vol. 14, p. 195.
[5] L.J.J. Janssen, in 'Modern Chlor-Alkali Technology', Ed. C. Jackson, Ellis Horwood Publishers, Chichester, 1983, Vol. 2, p. 271.
[6] J. Rolewicz, Ch. Comninellis, E. Plattner, J. Hinden, *Chimia* **1988**, *42*, 75.
[7] J. Rolewicz, Ch. Comninellis, E. Plattner, J. Hinden, *Electrochim. Acta* **1988**, *33*, 573.
[8] Ch. Comninellis, G.P. Vercesi, *J. Appl. Electrochem.* **1991**, *21*, 136.
[9] G.P. Vercesi, J. Rolewicz, Ch. Comninellis, J. Hinden, *Thermochim. Acta* **1991**, *176*, 31.
[10] G.P. Vercesi, J.-Y. Salamin, Ch. Comninellis, *Electrochim. Acta* **1991**, *36*, 991.
[11] Ch. Comninellis, G.P. Vercesi, *J. Appl. Electrochem.* **1991**, *21*, 335.
[12] A. Benedetti, S. Polizzi, P. Riello, A. De Battisti, A. Maldotti, *J. Mater. Chem.* **1991**, *1*, 511.
[13] A. De Battisti, A. Barbieri, A. Giatti, G. Battaglin, S. Daolio, A. Boscolo, *J. Mater. Chem.* **1991**, *1*, 191.
[14] M. Guglielmi, P. Colombo, V. Rigato, G. Battaglin, A. Boscolo, A. De Battisti, *J. Electrochem. Soc.* **1992**, *139*, 1655.
[15] G. Lodi, A. De Battisti, G. Bordin, C. De Asmundis, A. Benedetti, *J. Electroanal. Chem.* **1990**, *277*, 139.
[16] A.E. Newkirk, D.W. McKee, *J. Catal.* **1968**, *11*, 370.
[17] G.W. Jang, K. Rajeshwar, *J. Electrochem. Soc.* **1987**, *134*, 1830.
[18] G. Lodi, A. Benedetti, G. Fagherazzi, J. Kristof, *J. Electroanal. Chem.* **1988**, *256*, 441.
[19] Joint Commitee on Powder Diffraction Standards, Powder Diffraction File 15-870, International Centre for Diffraction Data, Swarthmore, PA, 1988.
[20] L. Lutterotti, P. Scardi, *J. Appl. Crystallogr.* **1990**, *23*, 246.
[21] G. Battaglin, A. De Battisti, A. Barbieri, A. Giatti, A. Marchi, *Surf. Sci.* **1991**, *251/252*, 73.
[22] L.D. Burke, O.J. Murphy, *J. Electroanal. Chem.* **1980**, *109*, 199.